# The NSUN2-YBX1 axis enhances m⁵C modification to facilitate NPM1-mediated nuclear translocation of PKM2, augmenting the Warburg effect and promoting nasopharyngeal carcinoma progression in a mouse model

Zhi Wang[1], Xubo Chen[1], Shuhong Wu[1], Bing Liao[1], Liqing Guo[1], Yuehui Liu[1], Tao Zhou[2]

The NSUN2-YBX1 axis enhances m⁵C modification to facilitate NPM-1 mediated nuclear translocation of PKM2, augmenting the Warburg effect and promoting nasopharyngeal carcinoma (NPC) progression in a mouse model

Wang Z, Chen X, Wu S et al.   Rhinology 2025.   https://doi.org/10.4193/Rhin24.496
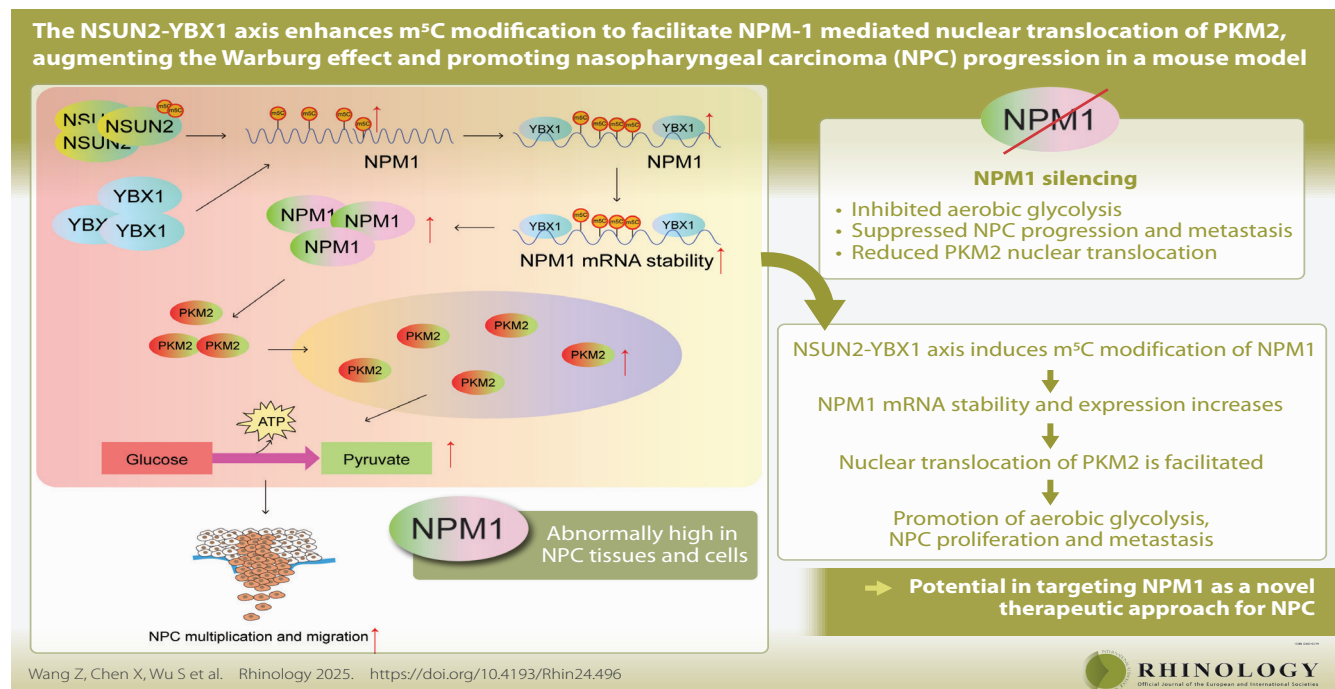
Abstract

Background: Nasopharyngeal carcinoma (NPC) is notable not only for its distinct geographic and ethnic distribution but also for its metabolic alterations. A key feature of NPC is its reliance on aerobic glycolysis for energy production. This shift from oxidative phosphorylation to glycolysis provides cancer cells with a metabolic advantage, supporting rapid growth and survival. Targeting aerobic glycolysis has therefore emerged as a promising therapeutic strategy. **Methods**: RT-qPCR, Western blot, IHC, and IF staining were used to examine gene and protein expression levels. Cell viability, proliferation, migration, and invasion were measured using the CCK-8 assay, colony formation assay, and transwell assay, respectively. Interactions among NPM1, PKM2, NSUN2, and YBX1 were examined using RIP, Co-IP, MeRIP, RNA pulldown, and dual-luciferase reporter assays. Aerobic glycolysis and oxidative phosphorylation (OXPHOS) levels were analyzed using the XF96 metabolic analyzer. Additionally, an in vivo mouse model of NPC was established for further validation. **Results**: NPM1 was abnormally elevated in NPC tissues and cells. Silencing of NPM1 inhibited aerobic glycolysis, suppressed NPC progression and metastasis, and reduced PKM2 nuclear translocation. Mechanistically, NPM1 physically interacted with PKM2 to promote its nuclear localization, while the NSUN2/YBX1 axis upregulated NPM1 expression through m⁵C modification, stabilizing NPM1 mRNA. **Conclusion**: The NSUN2-YBX1 axis induces m⁵C modification of NPM1, leading to increased NPM1 stability and its expression. This upregulation facilitates the nuclear translocation of PKM2, which promotes aerobic glycolysis and drives the proliferation and metastasis of NPC. These findings highlight the potential of targeting NPM1 as a novel therapeutic approach for NPC.

Key words: aerobic glycolysis, m⁵C modification, nasopharyngeal carcinoma (NPC), NPM1 (nucleophosmin 1), pyruvate kinase M2 (PKM2) translocation

Introduction

Nasopharyngeal carcinoma (NPC) is a malignant tumor originating from the epithelial cells of the nasopharynx, characterized by its unique geographic and ethnic prevalence [1]. It occurs at particularly high rates in southern China and Southeast Asia [2]. Radiotherapy is the primary treatment for NPC, often supplemented by chemotherapy, targeted therapy, immunotherapy, and surgery in a comprehensive therapeutic approach [3]. Despite these interventions, the high rates of recurrence and metastasis result in suboptimal treatment outcomes [3]. Therefore, understanding NPC's pathogenesis to identify new therapeutic targets is essential for reducing recurrence, limiting metastasis, and improving patient survival. While normally differentiated cells primarily generate energy through mitochondrial oxidative phosphorylation, most tumor cells, including NPC cells, rely on aerobic glycolysis, a metabolic shift commonly referred to as the "Warburg effect"[4]. In NPC, key enzymes involved in aerobic glycolysis are highly expressed, supporting a high metabolic rate and enabling the cells to produce more energy than they would through oxidative phosphorylation [5]. As a result, inhibiting aerobic glycolysis may be a critical strategy for alleviating NPC. Studies have shown that pyruvate kinase M2 (PKM2) plays a role in regulating tumor cell growth and promoting metabolic processes that produce lactate, thereby providing adenosine triphosphate (ATP) to meet the high metabolic demands of tumor cells [6]. PKM2 is thus a key protein driving tumor cells toward a high-energy metabolic state and is closely associated with poor prognosis in cancer patients [7]. PKM2 exists in three kinetic forms: monomer, dimer, and tetramer [8]. Both the dimeric and tetrameric forms of PKM2 possess kinase activity, but they function differently [9]. The dimeric form promotes the conversion of pyruvate into lactate through glycolysis, while the tetrameric form directs pyruvate into the tricarboxylic acid (TCA) cycle, contributing to oxidative phosphorylation and ATP production [10]. In tumor cells, PKM2 is primarily present in its dimeric form [6]. In this state, it is closely linked to the synthesis of nucleic acids and amino acids and can enter the nucleus to act as a transcription factor, activating genes associated with tumor growth [6]. Furthermore, research has shown that inhibiting the conversion of PKM2 from its tetrameric to dimeric state enhanced its pyruvate kinase activity and reduced its nuclear localization, and vice versa [11]. A study on NPC indicated that PKM2 expression was upregulated in NPC cells, promoting cell proliferation and metastasis [12]. Therefore, we speculated that increasing the nuclear localization of PKM2 in NPC cells could enhance aerobic glycolysis, thereby promoting the proliferation and metastasis of NPC cells.

Nucleophosmin (NPM1) is an essential cellular protein involved in several key biological processes, such as mRNA transport, chromatin remodeling, regulation of apoptosis, and maintenance of genome stability [13]. Its role is crucial for normal cellular function, as highlighted by its frequent overexpression, mutation, rearrangement, or occasional deletion in various cancers [13]. Analysis using the GEPIA database shows that NPM1 was highly expressed in head and neck squamous cell carcinoma, and this high expression was associated with poor patient prognosis. Previous studies also suggest that NPM1 was involved in regulating NPC [14]. For example, a study investigating drug-resistant genes in NPC suggests that NPM1 may be involved in radioresistance [14]. Another study indicates that NPM1 may also play a role in the metastasis of NPC [15]. Previous work by our group has demonstrated that NPM1 promoted NPC proliferation, invasion, and migration via the epidermal growth factor receptor-phosphoinositide 3-kinase/protein kinase B (EGFR-PI3K/AKT) signaling pathway. Furthermore, predictions from the STRING database suggest an interaction between NPM1 and PKM2. NPM1 is known to shuttle between the nucleus and cytoplasm through nuclear pores, participating in nuclear-cytoplasmic transport [16]. Based on these findings, we propose that NPM1 may bind to dimeric PKM2, facilitating its nuclear entry, thereby promoting NPC proliferation and metastasis.

5-Methylcytosine (m^{5}C) has been detected in messenger RNA (mRNA), ribosomal RNA (rRNA), and transfer RNA (tRNA) across various species [17]. As a reversible epigenetic modification, m^{5}C plays a crucial role in several biological processes, including the regulation of RNA stability, protein interactions, and transcriptional control [18]. The m^{5}C modification is mediated by three types of proteins: methyltransferases (writers), which catalyze the deposition of specific RNA modification sites; demethylases (erasers), which remove these modifications; and binding proteins (readers), which primarily recognize and bind to the modified sites [18]. Our analysis of NPM1 mRNA revealed a high level of m^{5}C modifications. Moreover, bioinformatics predictions suggest that Aly/REF export factor (ALYREF), a "reader" protein; NOP2/Sun RNA methyltransferase 2 (NSUN2) and NSUN6, which are "writer" proteins; and Y-box binding protein 1 (YBX1), another "reader" protein, can bind to the m^{5}C sites on NPM1 mRNA. Previous studies have shown that NSUN2 and YBX1 were highly expressed in NPC and promote their progression [19, 20]. However, the roles of NSUN2 and YBX1 in regulating NPM1 in NPC remain not entirely clear and need to be further investigated.

In conclusion, we hypothesized that NSUN2 enhanced the m^{5}C modification of NPM1, while YBX1 bound to the m^{5}C-modified NPM1 mRNA, thereby stabilizing it and increasing NPM1 expression. The elevated levels of NPM1 promoted the nuclear localization of PKM2, leading to enhanced aerobic glycolysis, proliferation, and metastasis in NPC.

Materials and methods

Most of the Materials and Methods are presented in the supplementary material.

m⁵C dot blot hybridization assay

Poly(A)+ mRNA was extracted from HK-1, C666-1, NP69, and CNE3 cells—either untransfected or transfected with shNSUN2 or shNC—using the Dynabeads™ mRNA DIRECT™ Purification Kit (ThermoFisher Scientific, Cat. No. 61011). The isolated mRNA was then diluted to an equal concentration in all samples using 10 mM Tris-HCl, as supplied with the kit. The mRNA was transferred onto a positively charged Nylon66 membrane (Biodyne B, 0.45 µm, Cat. No. 60209) and crosslinked twice with UV light at 1200 µJ using a UV Stratalinker 2400 (Stratagene). The membrane was then washed in 0.02% PBST for 10 minutes and incubated overnight at 4°C with an anti-m⁵C antibody (Abcam, Cat. No. ab214727) at a 1:100 dilution in 5% non-fat milk in 0.02% PBST. After incubation, the membrane was washed twice with 0.02% PBST for 10 minutes each, followed by treatment with a secondary antibody diluted 1:10,000 in 5% non-fat milk in 0.02% PBST. The membrane was then subjected to three additional washes with 0.02% PBST before being stained with 0.1% methylene blue (Sigma-Aldrich, Cat. No. M9140-25G) in 0.5 M ammonium acetate.

Statistical analysis

Data analysis was conducted using SPSS software, version 20.0 (IBM, Armonk, NY, USA). Results are presented as the mean ± standard deviation (SD) from a minimum of three independent experiments. Differences between the two groups were evaluated using an unpaired Student's t-test, while comparisons among more than two groups were assessed using one-way ANOVA followed by Tukey's post hoc test. Statistical significance was set at a p-value of less than 0.05. Additionally, the two-way ANOVA with Tukey's multiple comparison tests was employed to compare multiple groups across different time points.

Results

NPM1 was highly expressed in nasopharyngeal carcinoma tissues and cells

To investigate NPM1 expression in NPC, we first assessed its levels in NPC tissues. NPM1 was elevated in NPC tissues (Figure S1A). Consistent with these findings, NPM1 expression was elevated in NPC cell lines, including CNE3, HK-1, and C666-1, compared to the normal nasopharyngeal epithelial cell line NP69 (Figure S1B). Among these cell lines, HK-1 and CNE3 showed the highest expression of NPM1 and were selected for further studies. Taken together, NPM1 was abnormally upregulated in NPC.

NPM1 interacted with PKM2 to promote its nuclear translocation

We next investigated the mechanisms underlying NPM1-mediated regulation in NPC. BioGRID predictions indicated an interaction between NPM1 and PKM2 (Figure 1A). This interaction was further confirmed using Co-IP assays in NPC cell lines, HK-1 and

CNE3, and 293T cells, demonstrating that NPM1 and PKM2 physically bind to each other in NPC cells (Figure 1B-C). IF staining of the two NPC cell lines showed that NPM1 and PKM2 co-localized in both the cytoplasm and the nucleus (Figure 1D). Western blot analysis revealed that PKM2 was highly expressed in NPC cell lines (CNE3, HK-1, and C666-1) compared to NP69 cells (Figure 1E). Next, NPC cells with NPM1 knockdown (shNPM1) were generated in the HK-1 and CNE3 cell lines and compared with control cells (shNC). Western blot results confirmed a reduction in NPM1 expression in the knockdown cells (Figure 1F), and this was associated with reduced nuclear localization of PKM2 (Figure 1G-H). Altogether, these findings indicate that NPM1 bound to PKM2 and induced its nuclear translocation.

Knockdown of NPM1 suppressed nasopharyngeal carcinoma proliferation and metastasis

To assess the effects of NPM1 knockdown on NPC cell behavior, two NPC cell lines, HK-1 and CNE3, with NPM1 knockdown (shNPM1) and control cells (shNC) were examined. Knockdown of NPM1 led to a notable reduction in the viability, proliferation, invasion, and migration of HK-1 and CNE3 cells (Figure 2A-C). Subcutaneous injection of NPM1 knockdown cells into nude mice resulted in smaller tumors with reduced volume and weight compared to controls (Figure 2D-F). Immunohistochemistry analysis showed decreased NPM1 expression in the tumors of knockdown mice (Figure S2A). Additionally, tail vein injection of NPM1 knockdown cells into mice led to a marked decrease in lung metastasis and the number of nodules compared to control mice (Figure S2B-D). These results demonstrate that NPM1 knockdown inhibited NPC progression and metastasis.

NPM1 knockdown inhibited aerobic glycolysis in nasopharyngeal carcinoma cells

To investigate the impact of NPM1 knockdown on the metabolic activity of NPC cells, we first analyzed the ECAR and OCR levels in the NP69 and NPC cell lines (HK-1 and C666-1). The results showed that NPC cell lines exhibited elevated ECAR levels and decreased OCR levels compared to NP69 cells (Figure 3A). To further explore the role of NPM1, NPM1-knockdown NPC cell lines (shNPM1) and control cells (shNC) were established. ECAR analysis demonstrated a decrease in glycolytic activity, including reduced glycolytic capacity, basal glycolysis rate, and maximum glycolytic rate, upon NPM1 knockdown (Figure 3B). In contrast, OCR analysis revealed that NPM1 knockdown led to increased levels of OXPHOS, with elevated basal respiration, ATP production, maximal respiration, and spare respiratory capacity (Figure 3C). These findings suggest that NPM1 knockdown suppressed aerobic glycolysis while enhancing mitochondrial oxidative phosphorylation in NPC cells.
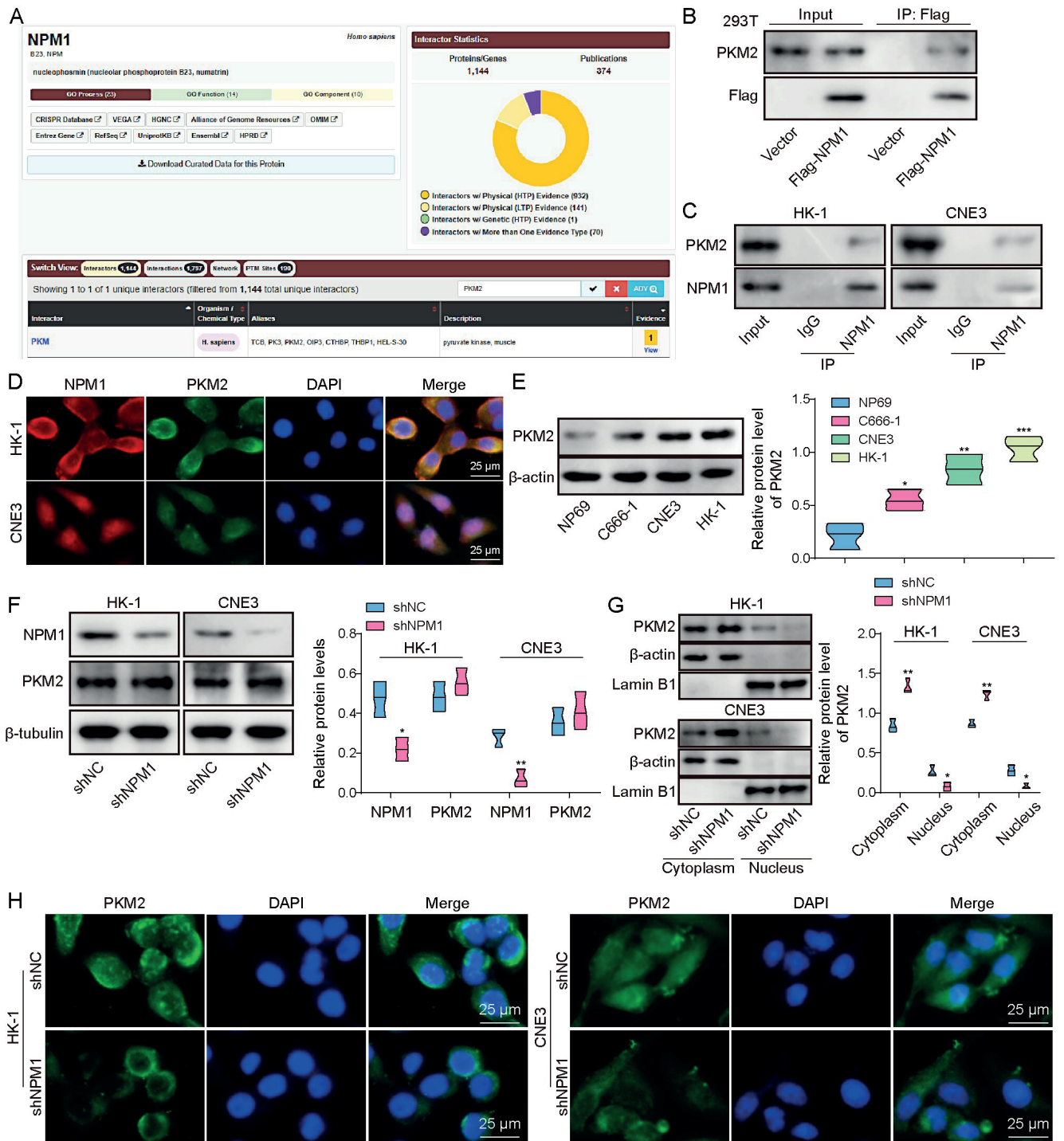
Figure 1. NPM1 interacted with PKM2 to promote its nuclear translocation. (A) The interaction between NPM1 and PKM2 was predicted using the BioGRID database. (B-C) Co-immunoprecipitation (Co-IP) was performed to detect the interaction between NPM1 and PKM2 in 293T cells, as well as in HK-1 and CNE3 cells. (D) Immunofluorescence (IF) was used to examine the colocalization of NPM1 and PKM2 in HK-1 and CNE3 cells. Scale bar = 25 μm. (E) Western blot analysis was used to assess the expression levels of PKM2 in the normal nasopharyngeal epithelial cell line (NP69) and NPC cell lines (CNE3, HK-1, and C666-1). HK-1 and CNE3 cells were transfected to create NPM1 knockdown cells, grouped into shNC (control) and shNPM1. (F) Western blot was performed to detect NPM1 and PKM2 expression. (G) Western blot was performed to analyze the cytoplasmic and nuclear levels of PKM2. (H) Immunofluorescence (IF) was also used to examine the localization of PKM2 within the cells. Scale bar = 25 μm. Data are presented as mean ± SD. n=3. *p<0.05, **p<0.01, ***p<0.001.
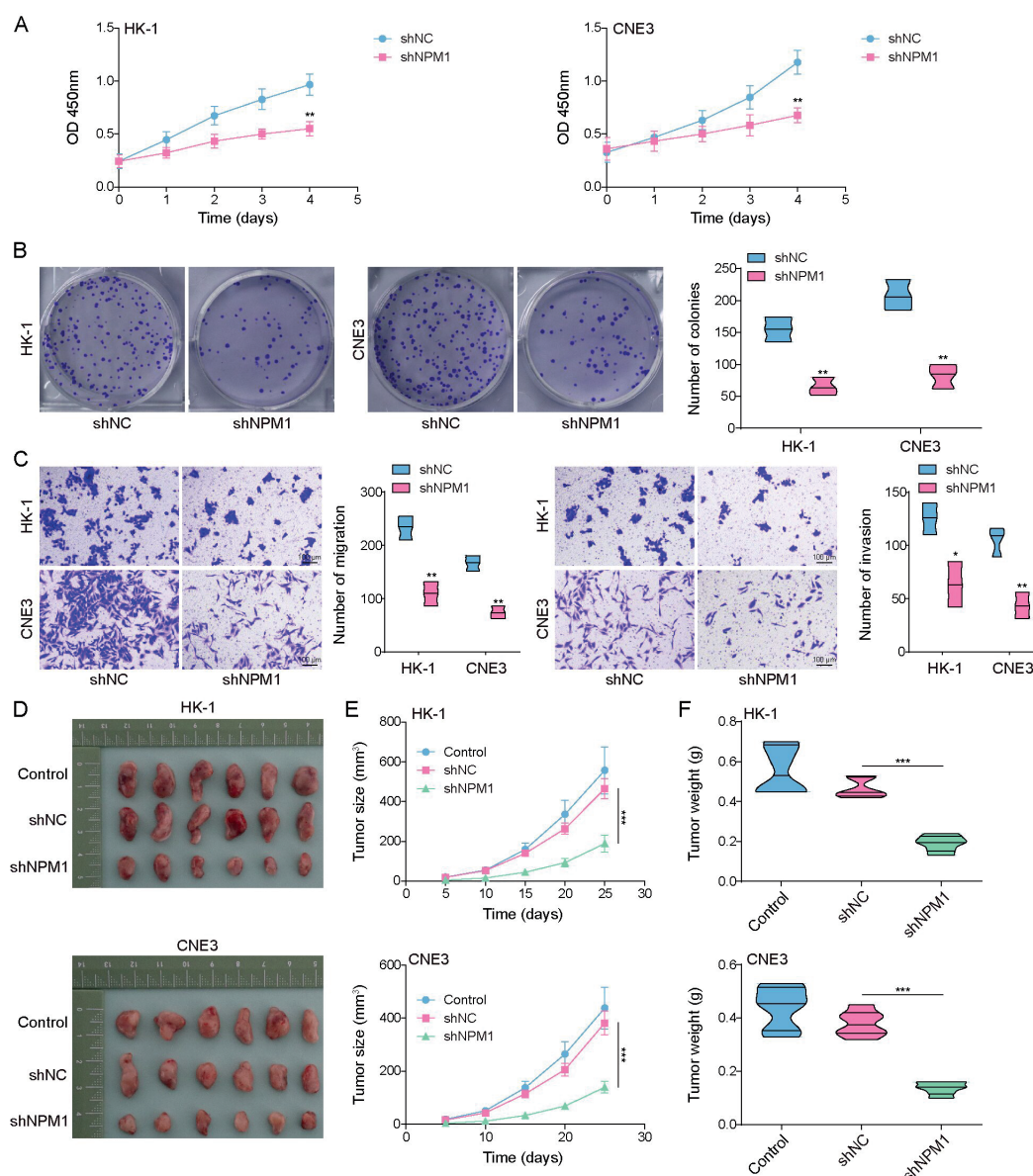
Figure 2. Knockdown of NPM1 suppressed nasopharyngeal carcinoma proliferation and metastasis. (A) Cell viability was assessed in NPM1-knockdown NPC cells (shNPM1) and control cells (shNC) using the CCK-8 assay. n=3. (B) Colony formation assays were conducted to evaluate the proliferative capacity of NPM1-knockdown and control NPC cells. n=3. (C) Invasion and migration of NPM1-knockdown and control NPC cells were measured using Transwell assays. Scale bar = 100 μm. n=3. (D-F) NPM1-knockdown and control NPC cells were subcutaneously injected into nude mice. Afterward, the tumor size, volume, and weight were examined. n=6. Data are presented as mean ± SD. *p<0.05, **p<0.01, ***p<0.001.

NSUN2 upregulated NPM1 levels via the m⁵C-YBX1 pathway

To further investigate the mechanism by which NPM1 mediates NPC, we utilized bioinformatics tools. RM2target identified NSUN2 as m⁵C writers associated with NPM1 (Figure 4A). Analysis of NPC tissues and adjacent normal tissues illustrated that NSUN2 was highly expressed in NPC tissues (Figure 4B), leading to the selection of NSUN2 for subsequent study. As expected, NSUN2 was found to be highly expressed in NPC cell lines (CNE3, HK-1, and C666-1) compared to NP69 cells (Figure 4C). Further analysis revealed increased overall m⁵C levels in NPC cells and elevated m⁵C modification on NPM1 mRNA (Figure 4D-E).

Subsequently, NSUN2 knockdown was carried out in two NPC cell lines, HK-1 and CNE3. This resulted in a reduction in NSUN2 expression, a decrease in overall m⁵C levels, and lower m⁵C modification on NPM1 mRNA (Figure 4F-H). Additional RIP and RNA pulldown assays confirmed that NSUN2 directly bound to NPM1 mRNA (Figure 4I-J). RM2target also predicted YBX1 and ALYREF as potential m⁵C readers interacting with NPM1 (Figure 4K). Both YBX1 and ALYREF were highly expressed in NPC cell lines (Figure 4L). Next, YBX1 and ALYREF were knocked down in HK-1 and CNE3 cells and the success of the knockdowns was validated by Western blot (Figure S3A). The dual-luciferase reporter assay
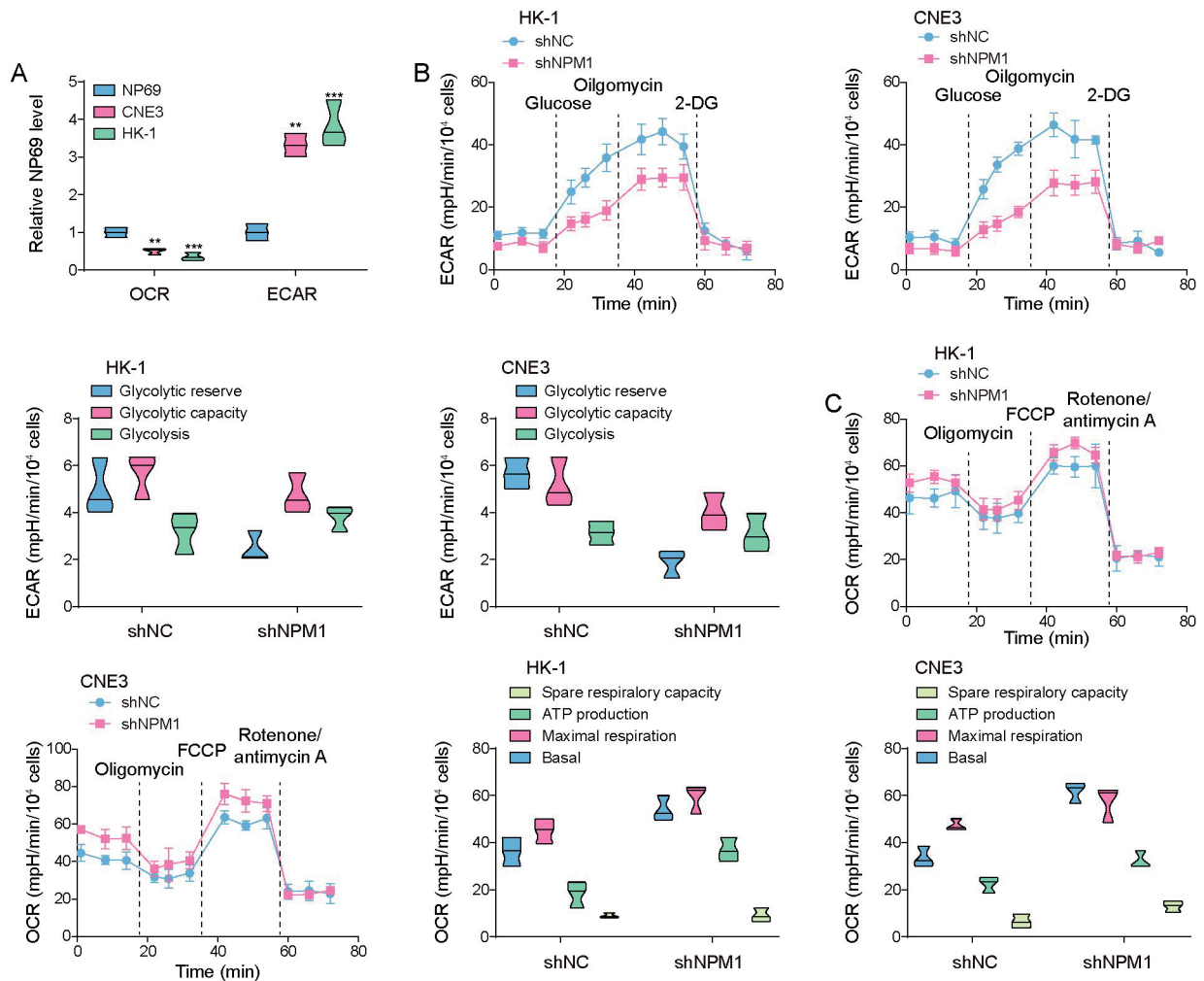
Figure 3. NPM1 knockdown inhibits aerobic glycolysis in nasopharyngeal carcinoma cells. (A) Extracellular acidification rate (ECAR) and oxygen consumption rate (OCR) were analyzed in the normal nasopharyngeal epithelial cell line (NP69) and NPC cell lines (HK-1 and CNE3). (B) ECAR analysis was performed using an XF96 metabolic analyzer to measure glycolytic changes, including glycolytic capacity, basal glycolysis rate, and maximum glycolysis rate, in NPM1-knockdown NPC cells (shNPM1) and control cells (shNC). (C) OCR analysis was conducted using an XF96 metabolic analyzer to assess levels of oxidative phosphorylation (OXPHOS), including basal respiration, maximal respiration, ATP production, and spare respiratory capacity, in NPM1-knockdown and control NPC cells. Data are presented as mean ± SD. n=3. **p<0.01, ***p<0.001.

demonstrated that YBX1 bound to NPM1 mRNA, while ALYREF did not (Figure S3B).

To further explore the roles of NSUN2 and YBX1, we created NPC cell lines with NSUN2 knockdown and/or YBX1 overexpression. NSUN2 knockdown reduced the expression of both NSUN2 and NPM1, while YBX1 overexpression increased the expression of YBX1 and NPM1, reversing the effects of NSUN2 knockdown on NPM1 expression (Figure S3C). NSUN2 knockdown accelerated actinomycin D-induced degradation of NPM1 mRNA in a time-dependent manner, while YBX1 overexpression had the opposite effect, counteracting the effect of NSUN2 knockdown (Figure S3D). Collectively, these findings suggest that NSUN2 upregulated NPM1 expression through m5C modification, with YBX1 acting as an m5C reader that stabilized NPM1 mRNA.

NSUN2 induced PKM2 nuclear translocation via NPM1, enhanced aerobic glycolysis, and facilitated the progression of nasopharyngeal carcinoma

To explore the role of NSUN2 and YBX1 in the regulation of PKM2 nuclear translocation, aerobic glycolysis, and NPC progression, two NPC cell lines, HK-1 and CNE3, were constructed with NSUN2 knockdown and/or YBX1 overexpression. NSUN2 knockdown led to a decrease in cell viability, proliferation, invasion, and migration, while YBX1 overexpression increased these capacities, effectively reversing the effects of NSUN2 knockdown (Figure 5A-C). Additionally, NSUN2 knockdown reduced the nuclear translocation of PKM2, whereas YBX1 overexpression promoted PKM2 nuclear localization, counteracting the effect of NSUN2 knockdown (Figure 5D). Metabolic analysis showed that NSUN2 knockdown resulted in decreased ECAR levels, indicating
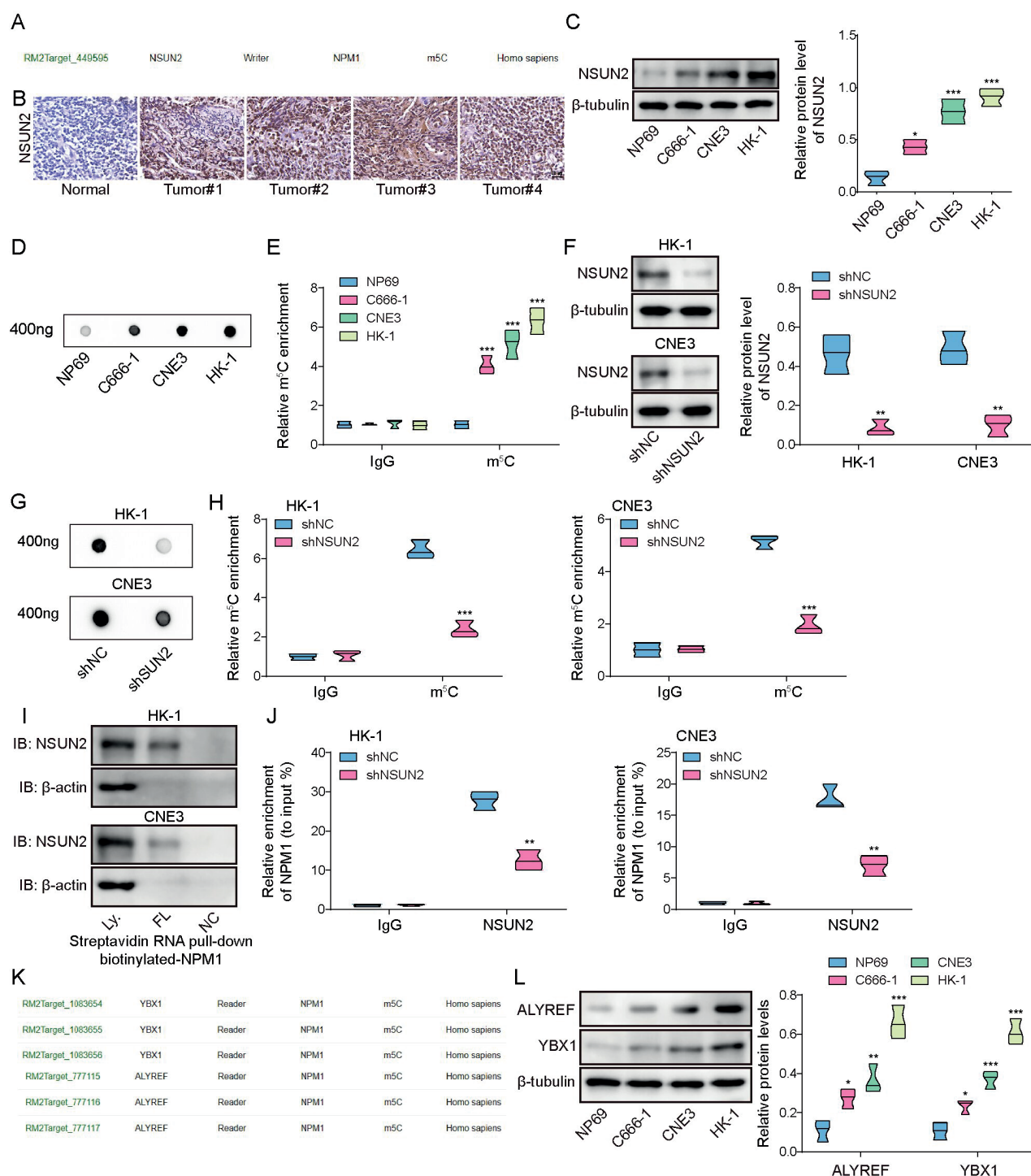
Figure 4. NSUN2 upregulated NPM1 levels via the m^{5}C-YBX1 pathway. (A) m^{5}C writers associated with NPM1 were predicted using RM2target. (B) Immunohistochemistry (IHC) was performed to assess the expression levels of NSUN2 in NPC tissues and adjacent normal tissues (n=5). Scale bar = 20 μm. (C) Western blot analysis was used to determine NSUN2 expression levels in the normal nasopharyngeal epithelial cell line (NP69) and NPC cell lines (CNE3, HK-1, and C666-1). (D) Dot blot hybridization was performed to measure overall m^{5}C levels in NPC cells. (E) Methylated RNA immuno-precipitation (meRIP) was used to detect m^{5}C modification levels on NPM1 mRNA. (F) Western blot analysis was used to confirm NSUN2 expression in NSUN2-knockdown NPC cell lines (shNSUN2) and control cells (shNC). (G) Dot blot hybridization was performed to assess changes in overall m^{5}C levels following NSUN2 knockdown. (H) meRIP was conducted to examine m^{5}C modification levels on NPM1 mRNA after NSUN2 knockdown. (I-J) RNA pulldown assays and RNA immunoprecipitation (RIP) were used to investigate the interaction between NSUN2 and NPM1 mRNA. (K) RM2target pre-dicted YBX1 and ALYREF as m^{5}C readers potentially interacting with NPM1. (L) Western blot analysis was performed to evaluate the expression levels of YBX1 and ALYREF in NP69 and NPC cell lines (CNE3, HK-1, and C666-1). Data are presented as mean ± SD. Unless specified otherwise, n=3 except for A-B and K. *p<0.05, **p<0.01, ***p<0.001.
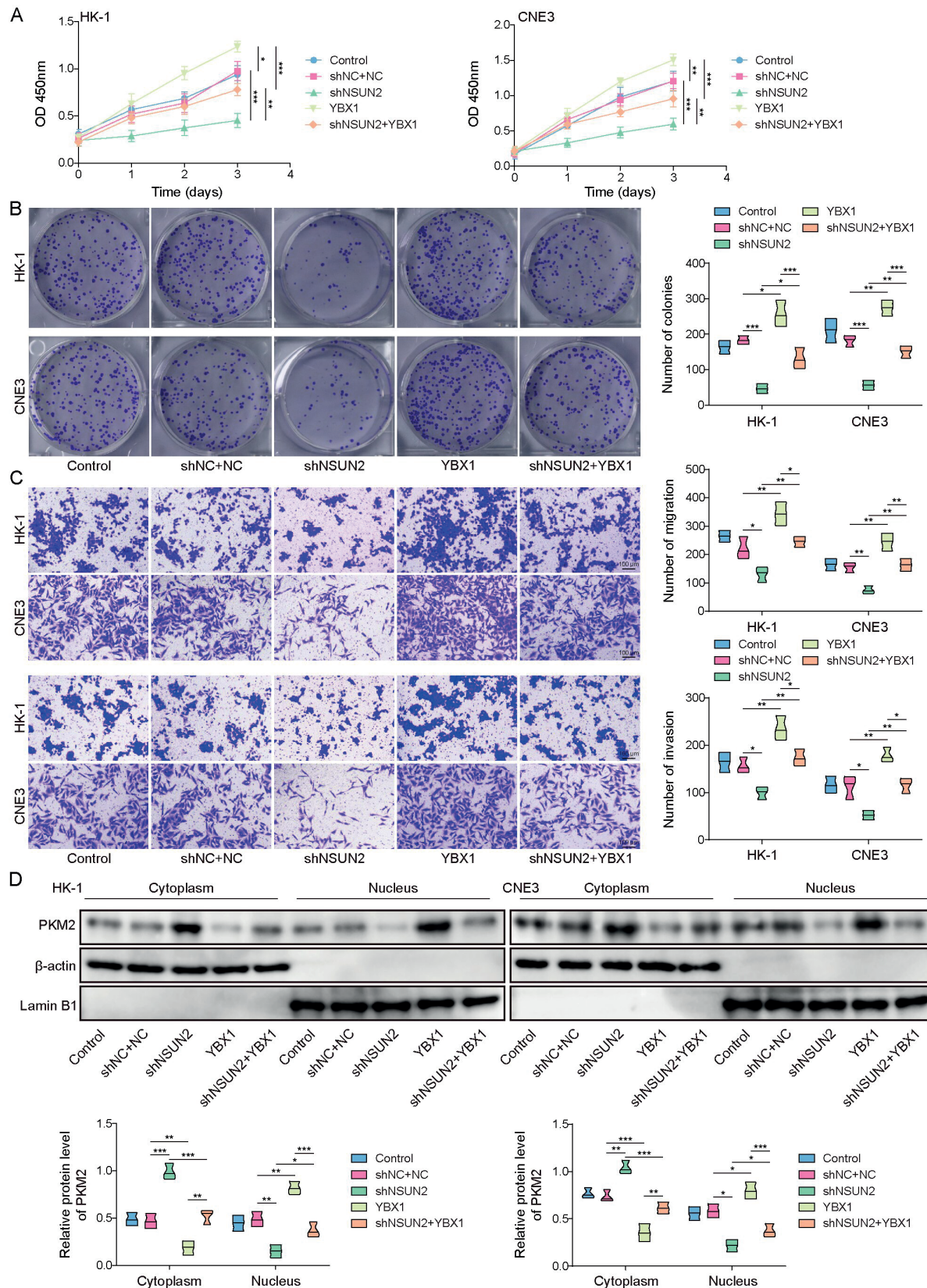
Figure 5. NSUN2 promotes PKM2 nuclear translocation via NPM1, enhances aerobic glycolysis, and facilitates the progression of nasopharyngeal carcinoma. (A) Cell viability was assessed in NPC cells with NSUN2 knockdown and/or YBX1 overexpression using the CCK-8 assay. (B) Colony formation assays were conducted to evaluate the proliferative capacity of NPC cells across the different groups. (C) Invasion and migration abilities of NPC cells were assessed using Transwell assays for each group. Scale bar = 100 μm. (D) Western blot analysis was performed to measure the expression levels of PKM2 in the cytoplasm and nucleus of NPC cells across the different groups. Data are presented as mean ± SD. n=3. *p<0.05, **p<0.01, ***p<0.001.
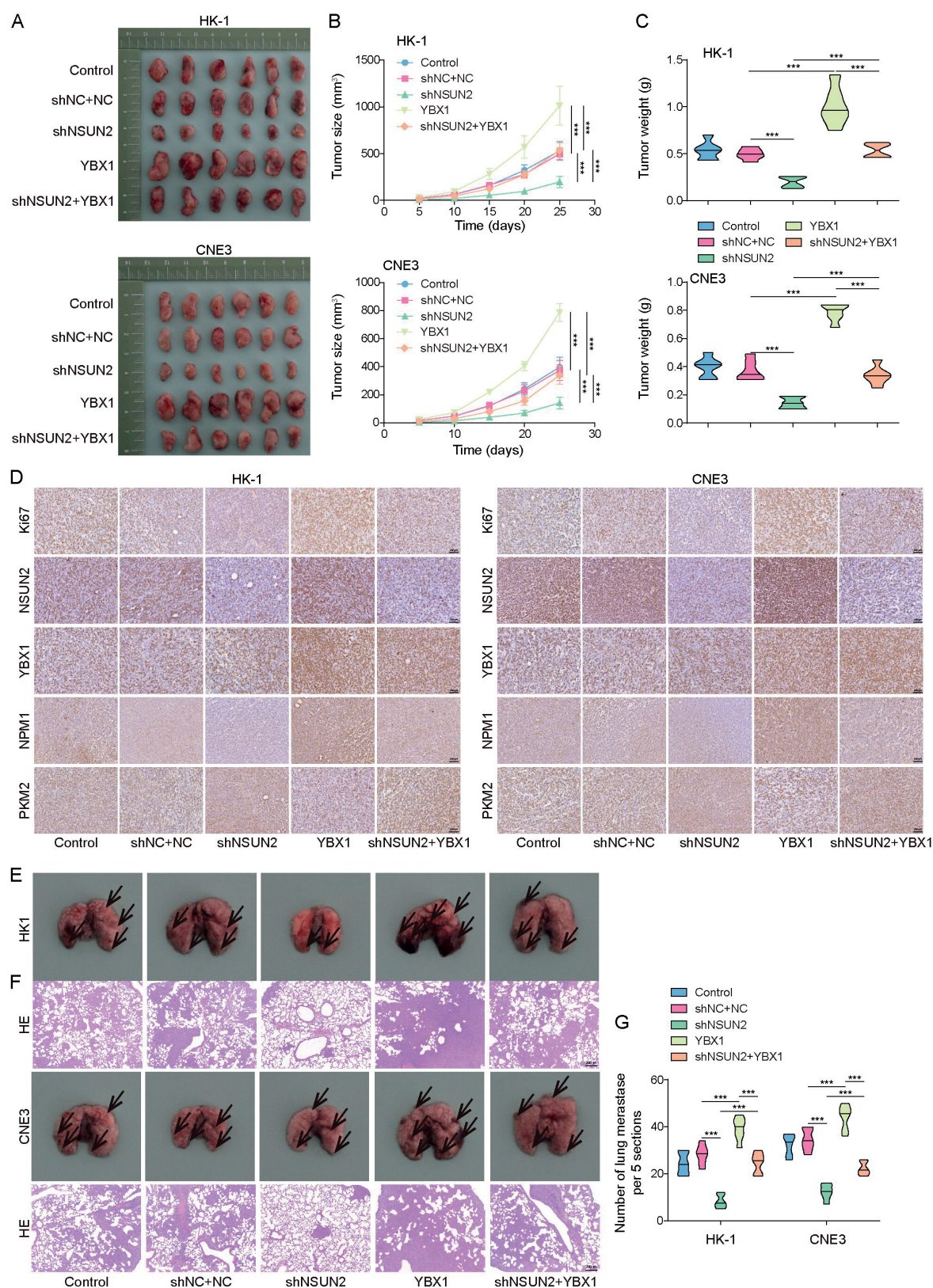
Figure 6. NSUN2 promoted the growth and metastasis of nasopharyngeal carcinoma tumors via YBX1/NPM1/PKM2 in vivo. (A-C) NPC cells with NSUN2 knockdown and/or YBX1 overexpression were subcutaneously injected into nude mice. Tumor size, volume, and weight were measured to evaluate the effects of different treatments. (D) Immunohistochemistry (IHC) was performed to detect the expression levels of Ki67, NSUN2, YBX1, NPM1, and PKM2 in the NPC tumor tissues obtained from the mice. Scale bar = 200 μm. (E-G) NPC cells with NSUN2 knockdown and/or YBX1 overexpression were injected via the tail vein into nude mice to evaluate lung metastasis. The number of lung metastases and nodules was observed and quantified. Scale bar = 200 μm. Data are presented as mean ± SD. n=6. ***p<0.001.

reduced glycolytic activity, while OCR levels increased, reflecting enhanced oxidative phosphorylation (Figure S4A-S4B). In contrast, YBX1 overexpression led to increased ECAR levels and decreased OCR levels, reversing the metabolic changes induced by NSUN2 knockdown. In summary, NSUN2 promoted PKM2 nuclear translocation and aerobic glycolysis, thereby enhancing NPC progression via NPM1.

NSUN2 promoted the growth and metastasis of nasopharyngeal carcinoma tumors via YBX1/NPM1/PKM2 in vivo
To examine the effects of NSUN2 knockdown and YBX1 overexpression on tumor growth and metastasis in NPC, HK-1, and CNE3 cells were constructed with NSUN2 knockdown and/or YBX1 overexpression. NSUN2 knockdown led to smaller tumors with reduced volume and weight, whereas YBX1 overexpression resulted in larger tumors with increased weight, reversing the effects of NSUN2 knockdown (Figure 6A-C). Immunohistochemistry analysis revealed that NSUN2 knockdown decreased the expression of Ki67, NSUN2, and NPM1, along with reduced nuclear expression of PKM2 (Figure 6D). In contrast, YBX1 overexpression increased the expression of Ki67, YBX1, and NPM1, as well as the nuclear expression of PKM2, counteracting the effects of NSUN2 knockdown on Ki67, NPM1 and the nuclear expression of PKM2. Additionally, intravenous injections of these cell lines into nude mice showed that NSUN2 knockdown led to reduced lung metastasis and fewer nodules, whereas YBX1 overexpression increased lung metastasis and the number of nodules, reversing the changes caused by NSUN2 knockdown (Figure 6E-G). In conclusion, NSUN2 knockdown suppressed NPC growth and metastasis via the YBX1/NPM1 axis.

Discussion

NPC is characterized not only by its distinct geographic and ethnic prevalence but also by its unique metabolic adaptations [21]. One of the hallmarks of NPC is the reliance on aerobic glycolysis for energy production [22]. This metabolic shift from oxidative phosphorylation to glycolysis confers a growth advantage on cancer cells, making aerobic glycolysis a potential therapeutic target [22]. Understanding this metabolic reprogramming is crucial for developing strategies to inhibit glycolytic pathways and improve treatment outcomes for NPC patients. In this study, we demonstrated that NPM1 was elevated in NPC. Knockdown of NPM1 suppressed aerobic glycolysis, thereby inhibiting NPC progression and metastasis. Additionally, we found that NPM1 interacted with PKM2 to promote its nuclear translocation, while the NSUN2/YBX1 axis induced NPM1 upregulation by enhancing the m5C modification of NPM1. These in vitro findings were further validated in an in vivo mouse model.
NPM1 plays a critical role in NPC progression by regulating multiple oncogenic pathways [15, 23]. For example, it promoted metastasis and cancer stemness by recruiting mouse double mi-

nute 2 homolog (Mdm2), leading to the ubiquitination-mediated degradation of tumor protein p53 (p53), thereby weakening tumor suppression mechanisms [15]. Furthermore, NPM1 was implicated in carcinogen-induced metastasis through the NPM1/ myelocytomatosis oncogene (c-Myc)/ N-Myc downstream-regulated gene 1 (NDRG1) axis, contributing to enhanced tumor aggressiveness [24]. Elevated NPM1 expression in drug-resistant NPC cell lines, such as cisplatin-resistant NPC cell line HONE1-CIS6, compared to non-resistant counterparts, underscores its involvement in therapy resistance [23]. Consistently, our findings revealed that NPM1 knockdown decreased NPC proliferation and metastasis by suppressing aerobic glycolysis. Additionally, we identified a novel interaction between NPM1 and PKM2, where NPM1 promoted the nuclear translocation of PKM2. Previous studies indicated that the translocation of PKM2 contributed to Warburg effects and cancer progression (25). The substitution of wild-type PKM2 with a nuclear translocation-deficient mutant inhibited the epidermal growth factor receptor (EGFR)-induced Warburg effect and suppressed brain tumor development in mice [26]. Nevertheless, to the best of our knowledge, we demonstrated that for the first time, NPM1 promoted NPC progression and metastasis by inducing PKM2 translocation into nuclear and thus aerobic glycolysis, suggesting a new mechanism by which NPM1 drives NPC progression.
NSUN2 is a widely studied RNA methyltransferase that mediates the m5C modification in both tRNA and mRNA, playing a crucial role in gene regulation [27]. Research has shown that NSUN2 facilitates the progression of several cancers by introducing m5C modifications to specific mRNAs, including hepatoma-derived growth factor (HDGF), LIN28 homolog B (LIN28B), phosphoribosylformylglycinamidine synthase (PFAS), TIAM Rac1-associated GEF 2 (TIAM2), cyclin-dependent kinase inhibitor 1C (p57Kip2), and fatty acid binding protein 5 (FABP5) in bladder cancer, esophageal squamous cell carcinoma, pancreatic cancer, retinoblastoma, gastric cancer, and osteosarcoma, respectively [28-33]. Moreover, YBX1, an established m5C-binding protein, worked with NSUN2 to stabilize HDGF mRNA in bladder cancer and to increase quiescin sulfhydryl oxidase 1 (QSOX1) mRNA translation in non-small-cell lung cancer. Another study reported that NSUN2 and YBX1 collaborated to modify enolase 1 (ENO1) mRNA, impacting metabolic reprogramming and enhancing glucose metabolism in colorectal cancer [34]. Additionally, NSUN2 interacted with nucleolar proteins like NPM1 and nucleolin in HeLa cells, although this interaction with NPM1 was disrupted during mitosis [35]. Consistent with these findings, our results showed that NSUN2 increased the m5C modification of NPM1 mRNA, and YBX1 subsequently bound to NPM1 mRNA, enhancing its stability and upregulating NPM1 expression. This suggests a coordinated role of NSUN2 and YBX1 in regulating NPM1 levels through m5C modification.
In summary, the NSUN2-YBX1 axis enhances m5C modification

of NPM1, increasing its mRNA stability and expression, which in turn promotes PKM2 nuclear translocation, boosts aerobic glycolysis, and drives NPC proliferation and metastasis. These findings have important clinical implications for managing NPC, especially in addressing metabolic reprogramming and therapy resistance. The discovery of the NSUN2-YBX1-NPM1 axis as a critical driver of aerobic glycolysis and tumor progression offers new opportunities for targeted therapies. Currently, NPC treatment relies heavily on radiotherapy and chemotherapy, with cisplatin as a key component (36). However, resistance to cisplatin and other treatments remains a significant challenge [37]. Our results suggest that targeting the NSUN2-YBX1-NPM1 pathway could help overcome resistance by disrupting the metabolic changes that support tumor growth. For example, small-molecule inhibitors or RNA-based therapies targeting NSUN2, YBX1, or NPM1 could be combined with existing treatments to improve their effectiveness. Preclinical studies in other cancers have shown promising results with similar approaches, such as targeting metabolic pathways to enhance chemotherapy efficacy [38]. Additionally, the increased levels of NPM1 in cisplatin-resistant NPC cells indicate its potential as a biomarker for predicting treatment response and guiding personalized therapy. Biomarker-driven strategies have been successfully implemented in other cancers, such as non-small-cell lung cancer and breast cancer, improving patient outcomes [39, 40]. Integrating these findings into clinical practice would require further validation in patient samples and clinical trials to ensure safety and efficacy. Combining metabolic inhibitors with current therapies could also enhance outcomes, particularly for patients with advanced or resistant diseases. For instance, combining glycolysis inhibitors with cisplatin has shown synergistic effects in preclinical models of head and neck cancers [41]. Overall, this study advances our understanding of NPC biology and lays the groundwork for new therapeutic strategies that could be integrated into current treatment approaches.

Conclusion

While our findings provide mechanistic insights into the role of NPM1 and its regulation by NSUN2/YBX1, the study primarily relied on in vitro experiments and mouse models. These models may not fully recapitulate the complexity of human NPC, particularly the tumor microenvironment, immune interactions, and metabolic heterogeneity. These models may not fully capture the complexity of human NPC, particularly in terms of tumor microenvironment interactions and immune responses. Future studies should focus on validating these results in clinical samples from diverse patient populations and investigate the long-term consequences of modulating this pathway. Furthermore, the precise mechanisms by which NPM1 promotes PKM2 nuclear translocation and how this process is regulated by m^5C modifications remain incompletely understood. Further

studies should explore the structural and functional interactions between NPM1 and PKM2, as well as the role of other potential co-factors or post-translational modifications that may influence this process. Additionally, targeting the NSUN2-YBX1-NPM1 pathway may have unintended consequences, as these molecules are involved in various cellular processes beyond NPC. Inhibiting these proteins could lead to off-target effects and toxicity. Further research is also needed to explore potential combination therapies that integrate metabolic and transcriptional targeting approaches to improve treatment outcomes while minimizing adverse effects.

Abbreviations

ALYREF: ALY/REF Export Factor; AKT: Protein Kinase B; ATP: Adenosine Triphosphate; BCA: Bicinchoninic Acid; CCK-8: Cell Counting Kit-8; CCCP: Carbonyl Cyanide m-Chlorophenyl Hydrazone; COIP: Co-immunoprecipitation; DMEM: Dulbecco's Modified Eagle Medium; ECL: Enhanced Chemiluminescence; ECAR: Extracellular Acidification Rate; EGFR: Epidermal Growth Factor Receptor; IF: Immunofluorescence; MERIP: Methylated RNA Immunoprecipitation; m5C: 5-Methylcytosine; mRNA: Messenger RNA; NPM1: Nucleophosmin 1; NSUN2: NOP2/Sun RNA Methyltransferase Family Member 2; NSUN6: NOP2/Sun RNA Methyltransferase Family Member 6; NPC: Nasopharyngeal Carcinoma; OCR: Oxygen Consumption Rate; OXPHOS: Oxidative Phosphorylation; PBS: Phosphate-Buffered Saline; PI3K: Phosphoinositide 3-Kinase; PKM2: Pyruvate Kinase M2; PVDF: Polyvinylidene Fluoride; RIPA: Radioimmunoprecipitation Assay; RIP: RNA Immunoprecipitation; rRNA: Ribosomal RNA; RT-qPCR: Reverse Transcription-Quantitative Polymerase Chain Reaction; SDS-PAGE: Sodium Dodecyl Sulfate-Polyacrylamide Gel Electrophoresis; shNC: Short Hairpin Non-targeting Control; shRNA: Short Hairpin RNA; SPSS: Statistical Package for the Social Sciences; STRING: Search Tool for the Retrieval of Interacting Genes/Proteins; tRNA: Transfer RNA; YBX1: Y-Box Binding Protein 1.

Ethics approval and consent to participate

The animal experiments were approved by the Ethics Committee of The Second Affiliated Hospital of Nanchang University. The informed consent obtained from study participants.

Acknowledgements and Funding

Authorship contribution

ZW and TZ designed this study. ZW, XC, SW, BL, LG and YL collected the materials and performed the experiments. ZW analysed the data and wrote the manuscript. TZ revised the manuscript. All authors read and approved the final version of the manuscript.

Conflict of interest

No conflicts of interest, financial or otherwise, are declared by the authors.

References

1. Jicman Stan D, Niculet E, Lungu M, et al. Nasopharyngeal carcinoma: A new synthesis of literature data (Review). Exp Ther Med. 2022;23(2):136.
2. Cao SM, Simons MJ, Qian CN. The prevalence and prevention of nasopharyngeal carcinoma in China. Chin J Cancer. 2011;30(2):114-9.
3. Xu JY, Wei XL, Wang YQ, Wang FH. Current status and advances of immunotherapy in nasopharyngeal carcinoma. Ther Adv Med Oncol. 2022;14:17588359221096214.
4. Vander Heiden MG, Cantley LC, Thompson CB. Understanding the Warburg effect: the metabolic requirements of cell proliferation. Science. 2009;324(5930):1029-33.
5. Sung W-W, Chen P-R, Liao M-H, Lee J-W. Enhanced aerobic glycolysis of nasopharyngeal carcinoma cells by Epstein-Barr virus latent membrane protein 1. Exp Cell Res. 2017;359(1):94-100.
6. Zahra K, Dey T, Ashish, Mishra SP, Pandey U. Pyruvate Kinase M2 and cancer: the role of pkm2 in promoting tumorigenesis. Front Oncol. 2020;10:159.
7. Chiavarina B, Whitaker-Menezes D, Martinez-Outschoorn UE, et al. Pyruvate kinase expression (PKM1 and PKM2) in cancer-associated fibroblasts drives stromal nutrient production and tumor growth. Cancer Biol Ther. 2011;12(12):1101-13.
8. Wang P, Sun C, Zhu T, Xu Y. Structural insight into mechanisms for dynamic regulation of PKM2. Protein Cell. 2015;6(4):275-87.
9. Zhang Z, Deng X, Liu Y, Liu Y, Sun L, Chen F. PKM2, function and expression and regulation. Cell Biosci. 2019;9:52.
10. Wong N, De Melo J, Tang D. PKM2, a central point of regulation in cancer metabolism. Int J Cell Biol. 2013;2013:242513.
11. Chen X, Chen S, Yu D. Protein kinase function of pyruvate kinase M2 and cancer. Cancer Cell Int. 2020;20(1):523.
12. Zhao P, Zhou M, Chen R, Su R. Suppressed "Warburg Effect" in nasopharyngeal carcinoma via the inhibition of pyruvate kinase type M2-mediated energy generation pathway. Technol Cancer Res Treat. 2020;19:1533033820945804.
13. Box JK, Paquet N, Adams MN, et al. Nucleophosmin: from structure and function to disease development. BMC Molecular Biology. 2016;17(1):19.
14. Li Z, Li N, Shen L, Fu J. Quantitative proteomic analysis identifies MAPK15 as a potential regulator of radioresistance in nasopharyngeal carcinoma cells. Front Oncol. 2018;8:548.
15. Hu L, Gong P, Zhou N, et al. NPM1 promotes nasopharyngeal carcinoma metastasis and stemness by recruiting Mdm2 to induce the ubiquitination-mediated degradation of p53. Am J Cancer Res. 2023;13(5):1766-85.
16. Cela I, Di Matteo A, Federici L. Nucleophosmin in its interaction with ligands. Int J Mol Sci. 2020;21(14).
17. Gao Y, Fang J. RNA 5-methylcytosine modification and its emerging role as an epitranscriptomic mark. RNA Biol. 2021;18(sup1):117-27.
18. Song H, Zhang J, Liu B, et al. Biological roles of RNA m(5)C modification and its implications in Cancer immunotherapy. Biomark Res. 2022;10(1):15.
19. Tong X, Xiang Y, Hu Y, et al. NSUN2 promotes tumor progression and regulates immune infiltration in nasopharyngeal carcinoma. Front Oncol. 2022;12:788801.
20. Ban Y, Tan Y, Li X, et al. RNA-binding protein YBX1 promotes cell proliferation and invasiveness of nasopharyngeal carcinoma cells via binding to AURKA mRNA. Journal of Cancer. 2021;12(11):3315-24.
21. Zhang SQ, Pan SM, Liang SX, Han YS, Chen HB, Li JC. Research status and prospects of biomarkers for nasopharyngeal carcinoma in the era of high-throughput omics (Review). Int J Oncol. 2021;58(4).
22. Huang H, Li S, Tang Q, Zhu G. Metabolic reprogramming and immune evasion in nasopharyngeal carcinoma. Front Immunol. 2021;12:680955.
23. Sekhar KR, Freeman ML. Nucleophosmin plays a role in repairing DNA damage and is a target for cancer treatment. Cancer Research. 2023;83(10):1573-80.
24. Jia Q, Deng H, Wu Y, He Y, Tang F. Carcinogen-induced super-enhancer RNA promotes nasopharyngeal carcinoma metastasis through NPM1/c-Myc/NDRG1 axis. Am J Cancer Res. 2023;13(8):3781-98.
25. Yang W, Lu Z. Nuclear PKM2 regulates the Warburg effect. Cell Cycle. 2013;12(19):3154-8.
26. Yang W, Zheng Y, Xia Y, et al. ERK1/2-dependent phosphorylation and nuclear translocation of PKM2 promotes the Warburg effect. Nat Cell Biol. 2012;14(12):1295-304.
27. Chellamuthu A, Gray SG. The RNA methyltransferase NSUN2 and its potential roles in cancer. Cells. 2020;9(8).
28. Chen X, Li A, Sun BF, et al. 5-methylcytosine promotes pathogenesis of bladder cancer through stabilizing mRNAs. Nat Cell Biol. 2019;21(8):978-90.
29. Su J, Wu G, Ye Y, et al. NSUN2-mediated RNA 5-methylcytosine promotes esophageal squamous cell carcinoma progression via LIN28B-dependent GRB2 mRNA stabilization. Oncogene. 2021;40(39):5814-28.
30. Yang M, Wei R, Zhang S, et al. NSUN2 promotes osteosarcoma progression by enhancing the stability of FABP5 mRNA via m(5)C methylation. Cell Death Dis. 2023;14(2):125.
31. Mei L, Shen C, Miao R, et al. RNA methyltransferase NSUN2 promotes gastric cancer cell proliferation by repressing p57(Kip2) by an m(5)C-dependent manner. Cell Death Dis. 2020;11(4):270.
32. Zuo S, Li L, Wen X, et al. NSUN2-mediated m(5) C RNA methylation dictates retinoblastoma progression through promoting PFAS mRNA stability and expression. Clin Transl Med. 2023;13(5):e1273.
33. Zhang G, Liu L, Li J, et al. NSUN2 stimulates tumor progression via enhancing TIAM2 mRNA stability in pancreatic cancer. Cell Death Discov. 2023;9(1):219.
34. Chen B, Deng Y, Hong Y, et al. Metabolic recoding of NSUN2-mediated m(5)C modification promotes the progression of colorectal cancer via the NSUN2/YBX1/m(5)C-ENO1 Positive Feedback Loop. Adv Sci (Weinh). 2024;11(28):e2309840.
35. Sakita-Suto S, Kanda A, Suzuki F, Sato S, Takata T, Tatsuka M. Aurora-B regulates RNA methyltransferase NSUN2. Mol Biol Cell. 2007;18(3):1107-17.
36. Zhang L, Chen QY, Liu H, Tang LQ, Mai HQ. Emerging treatment options for nasopharyngeal carcinoma. Drug Des Devel Ther. 2013;7:37-52.
37. Xu H, Yin Q, Fan L, et al. RNF138 contributes to cisplatin resistance in nasopharyngeal carcinoma cells. Sci Rep. 2025;15(1):1406.
38. Luo Z, Eichinger KM, Zhang A, Li S. Targeting cancer metabolic pathways for improving chemotherapy and immunotherapy. Cancer Lett. 2023;575:216396.
39. AlDoughaim M, AlSuhebany N, AlZahrani M, et al. Cancer Biomarkers and Precision Oncology: A Review of Recent Trends and Innovations. Clin Med Insights Oncol. 2024;18:11795549241298541.
40. Slamon DJ, Leyland-Jones B, Shak S, et al. Use of chemotherapy plus a monoclonal antibody against HER2 for metastatic breast cancer that overexpresses HER2. N Engl J Med. 2001;344(11):783-92.
41. Kumar D. Regulation of glycolysis in head and neck squamous cell carcinoma. Postdoc J. 2017;5(1):14-28.

Tao Zhou
Department of Thyroid Surgery
The Second Affiliated Hospital
Jiangxi Medical College
Nanchang University
No.1, Minde Road
Donghu District
Nanchang 330000
Jiangxi Province
P.R. China

E-mail: Zhoutao903@126.com
Tel: +86-13397913215

Zhi Wang[1], Xubo Chen[1], Shuhong Wu[1], Bing Liao[1], Liqing Guo[1], Yuehui Liu[1], Tao Zhou[2]

[1] Department of Otorhinolaryngology Head and Neck Surgery, The Second Affiliated Hospital, Jiangxi Medical College, Nanchang University, Nanchang, Jiangxi Province, P.R. China

[2] Department of Thyroid Surgery, The Second Affiliated Hospital, Jiangxi Medical College, Nanchang University, Nanchang, Jiangxi Province, P.R. China

This manuscript contains online supplementary material

SUPPLEMENTARY MATERIAL

Supplementary Methods

Cell culture

The human nasopharyngeal epithelial cell line (NP69) and NPC cell lines (C666-1, CNE3, and HK1) were obtained from the Whelab (Shanghai China). NP69 cells were cultured in a keratinocyte serum-free medium (Invitrogen, CA, USA, Cat. No. MEPI-500CA) supplemented with Keratinocyte-SFM Growth Supplement and 2% fetal bovine serum (FBS, Gibco, Carlsbad, CA, USA, Cat. No. 12483020). The NPC cell lines, including CNE3, C666-1, and HK1, were maintained in RPMI 1640 medium (Invitrogen, Cat. No. C11875500BT) supplemented with 10% FBS. All cells were cultured at 37℃ in a humidified incubator with 5% CO_2.

Cell transfection

To investigate the effects of gene silencing and overexpression on NPC cells, we performed a series of transfection and infection experiments. NPC cells were added into 6-well plates and adhered for 24 hours before transfection. Short hairpin RNAs (shRNAs) specifically targeting NPM1 (shNPM1), NSUN2 (shNSUN2), YBX1 (shYBX1), and ALYREF (shALYREF), as well as a non-targeting control (shNC), were synthesized by Genesee Biotech and inserted into GV102 vectors (Genepharma, Shanghai, China). For overexpression studies, full-length YBX1 cDNA was amplified by PCR and cloned into the pcDNA3.1 vector (Promega, Madison, WI, USA), generating the YBX1 expression plasmid. An empty pcDNA3.1 vector served as the control (NC).

Transfections were carried out using 20 µL of Lipofectamine 3000 (Invitrogen) per well for a total of 5×10^6 cells. After 6 hours, the transfection medium was replaced with a fresh culture medium, and cells were incubated for an additional 48 hours to allow for gene expression. These transfected cells were subsequently used for in vitro functional assays to evaluate cell behavior.

To establish stable knockdown and overexpression cell lines, 293T cells (5×10^6 cells per well) were transfected with shNSUN2 alone, shNSUN2 combined with an YBX1- overexpressing lentivirus, or with control lentiviral vectors carrying either shNC or an empty vector (NC), using Lipofectamine 3000. After 48 hours, the virus-containing supernatants were collected, filtered, and used to infect HK-1 or CNE3 cells (5×10^6 cells per well). Infected cells were selected in 2.5 µg/mL puromycin for 12 days to ensure stable incorporation of the lentiviral constructs. After the selection process, puromycin was removed, and cells were allowed to recover in a standard culture medium until they reached full confluence.

Cell counting kit-8 (CCK-8) assay

To evaluate the proliferation of NPC cells, the CCK-8 assay (ab228554, Abcam, Cambridge, UK) was employed. Cells were plated in a 96-well plate at a density of 5,000 cells per well. After 48 hours, 10 µL of CCK-8 solution was added to each well. The cells were then incubated for 0, 1, 2, 3, and 4 hours, after which the absorbance
was measured using a microplate reader (Thermo Fisher Scientific, Männedorf, Switzerland).

Colony formation assay

NPC cells were treated as mentioned above. Afterward, the culture medium was replaced with fresh medium, and the cells were allowed to grow for an additional 7 days. The cells were subsequently fixed with 4% paraformaldehyde (PFA) for 15 minutes, rinsed three times with PBS, and stained with 10% methylene blue (Sigma- Aldrich, St. Louis, MI, USA). Colonies containing more than 50 cells were counted using a BZ-9000 Series microscope (Keyence, Itasca, IL, USA).

Transwell migration and invasion assay

For the migration assay, 20,000 cells were seeded into the upper compartment of a Transwell chamber with an 8 µm pore membrane (Corning Inc., Shanghai, China). For the invasion assay, a Matrigel-coated Transwell insert (BD Biosciences, San Jose, CA, USA) was used. Serum-free medium was added to the upper chamber, while the lower chamber contained medium supplemented with serum as a chemoattractant. After 48 hours of incubation, non-migrated cells on the upper surface of the membrane were carefully removed. Cells that had migrated or invaded to the lower surface were stained with crystal violet and observed under a DMi8 optical microscope (Zeiss, Jena, Germany).

Western blot

Proteins were extracted from cell samples by incubating them in radioimmunoprecipitation assay (RIPA) buffer containing a cocktail of protease inhibitors for 30 minutes at 4℃ (Beyotime Inc., Haimen, Jiangsu, China). The total protein content of each sample was determined using the bicinchoninic acid (BCA) protein assay kit (Thermo Fisher Scientific, Cat. No. 10741395). Equal amounts of protein (30 µg per sample) were separated by sodium dodecyl sulfate-polyacrylamide gel electrophoresis (SDS-PAGE) and transferred onto polyvinylidene fluoride (PVDF) membranes. The membranes were blocked and rinsed with PBS, followed by incubation with primary antibodies against NPM1 (1:500, Abcam, Cat. No. ab86712), PKM2 (1:1000, Abcam, Cat. No. ab85555), NSUN2 (1:1000, Abcam, Cat. No.

ab259941), ALYREF (1:1000, Thermo Fisher Scientific, Cat. No. H00010189-M03), YBX1 (1:1000, Abcam, Cat. No. ab255606), β-tubulin (1:1000, Abcam, Cat. No. ab6046), Lamin B1 (1:1000, Abcam, Cat. No. ab16048), and β-actin (1:1000, Abcam, Cat. No. ab8226). After washing with PBS, the membranes were treated with secondary antibodies (1:2000, Invitrogen, Cat. No. 31402). Protein bands were visualized using an enhanced chemilumi-nescence (ECL) detection system (Merck Millipore, Billerica, USA, Cat. No. WBULS0100).

qPCR
Total RNA was extracted from cells using Trizol reagent (Invi-trogen) following the manufacturer's instructions. A total of 1 µg of isolated RNA was reverse transcribed into complementary DNA (cDNA) using the PrimeScript cDNA Synthesis Kit (Takara, Osaka, Japan). Quantitative PCR (qPCR) was performed using the TaqMan® Universal PCR Master Mix (Thermo Fisher Scien-tific, Cat. No. 4305719) to amplify the target genes. The specific primers used for the reactions are listed in Table S1. Relative RNA expression levels were calculated using the 2-ΔΔCt method. GAPDH was used as the internal control for normalization.

Sample collection
For this study, the chip containing NPC tissues and normal tissues (cat. no. NPC1507) were purchased form Aijia biology (Changsha, Hunan). The tissue samples were stored in liquid nitrogen for subsequent experimental use.

Dual-luciferase reporter assay
The wild-type NPM1 (NPM1-wt) and its corresponding mutant version (NPM1-mut) were cloned into the psiCHECK2 vector (Promega) following PCR amplification. 293T cells were sub-sequently transfected with either the NPM1-wt or NPM1-mut constructs in combination with shALYREF, shYBX1, or their res-pective control shRNAs, using Lipofectamine 3000 (Invitrogen) to facilitate transfection. After 48 hours of incubation, luciferase activity was detected using a Dual-Luciferase Reporter Assay Kit (Promega) to evaluate the effects of the constructs and shRNA treatments.

Co-immunoprecipitation (Co-IP) assay
HK-1 and CNE3 cells were washed with ice-cold PBS and lysed in NP-40 buffer containing a protease inhibitor cocktail. The lysates were incubated on ice for 15 minutes, followed by centrifuga-tion at 15,000 g for 15 minutes to remove insoluble debris. The cleared supernatants were pre-cleared with protein G-Sepha-rose at 4°C for 15 minutes to reduce nonspecific binding. The samples were then incubated overnight at 4°C with an anti-NPM1 antibody (Thermo Fisher Scientific, 1:50, Cat. No. 32-5200) or a control IgG antibody (Abcam, 1:1000, Cat. No. ab18413). The following day, the immune complexes were captured by

incubating with protein G-Sepharose beads for an additional 2 hours at 4°C. The beads were washed four times with lysis buffer, resuspended in 4X loading buffer, and boiled for 5 minutes to denature the proteins. The samples were separated by SDS-PAGE and transferred onto a nitrocellulose membrane, then immunoblotted with primary antibodies against PKM2 or NPM1. 293T cells were transfected with Flag-tagged PKM2 and then were collected and lysed utilizing RIP lysis buffer (Millipore, USA). The lysates were incubated at 4°C overnight with an anti-Flag antibody or a control IgG to capture the target proteins through immunoprecipitation. The precipitated protein com-plexes were then isolated using a Co-IP Kit (Absin, China, Cat. No. abs955). Finally, the samples were analyzed by Western blot to assess the presence of the desired proteins.

RNA immunoprecipitation (RIP) assay
To perform the RNA RIP assay, HK-1, and CNE3 cells transfected with either shNSUN2 or shNC were processed using the EZ-Magna RIP RNA-Binding Protein Immunoprecipitation Kit (Merck Millipore, Cat. No. 17-701). The cells were lysed in RIP lysis buffer, and the lysates were subjected to sonication and centrifugation to obtain a clear supernatant. This supernatant was pre-cleared with magnetic beads before being incubated overnight at 4°C with an anti-NSUN2 antibody (Thermo Fisher Scientific, Cat. No. MA1-26754) or a control IgG antibody (Thermo Fisher Scientific, Cat. No. 20854-1-AP, 1:50 dilution). Post-incubation, RNA-protein complexes were captured using protein G Sepharose 4 Fast Flow beads (GE Amersham, Little Chalfont, UK). The complexes were then treated with proteinase K (Sangon, Shanghai, China) for 1 hour to release the RNA, which was subsequently purified and analyzed by qPCR following the qRT-PCR protocol using specific primers.

RNA pull-down assay
To isolate biotin-labeled RNA complexes, cell lysates from HK-1 and CNE3 cells were incubated with streptavidin-coated magne-tic beads, which bind specifically to biotin- tagged RNA, as per the manufacturer's protocol (Invitrogen). The lysates were mixed with custom biotinylated probes that specifically target NPM1 (GenePharma) to facilitate the capture of the desired RNA-protein interactions. After incubation, the beads were washed thoroughly to remove any proteins that were not specifically bound. The interaction between NPM1 and NSUN2 was subse-quently analyzed by Western blot.

Methylated RNA Immunoprecipitation (MeRIP)
Total RNA was extracted from NPC cells, and mRNA was subse-quently fragmented into approximately 100-nucleotide frag-ments using RNA Fragmentation Reagents (Invitrogen, AM8740). Around 400 ng of these fragmented mRNAs were incubated in immunoprecipitation (IP) buffer with 2.5 µg of anti-m5C

antibody (Abcam, 1:500, Cat. No. ab10805) or anti-IgG antibody (Merck Millipore, 1:500, Cat. No. AP113) at 25°C for 1 hour, under constant rotation. After incubation, the samples were washed with IP buffer, eluted, and precipitated using ethanol. The levels of m5C-modified mRNA were assessed by RNA extraction and subsequent analysis via RT-qPCR.

RNA stability assay

To evaluate RNA stability, HK-1, and CNE3 cells were transfected with either no construct, shNC along with NC, shNSUN2, YBX1, or a combination of shNSUN2 and YBX1. The cells were then treated with 5 µg/mL actinomycin D (Aladdin, Shanghai, China) for different time intervals (0, 4, and 8 hours). At each specified time point, the mRNA levels of NPM1 were measured using qPCR.

Animal studies

The animal experiments were approved by the Ethics Committee of The Second Affiliated Hospital of Nanchang University. Male BALB/C nude mice, aged between
four to six weeks, were obtained from Hunan SJA Laboratory Animal (Changsha, Hunan, China) and housed in a controlled environment.
For Figure 3, 36 mice were randomly divided into three groups: control, shNC, and shNPM1. HK-1 or CNE3 cells infected without (control) or with adenovirus-carrying shNC or shNPM1 were subcutaneously injected into the right flank of each mouse (1×106 cells in 200 µL PBS per mouse). Tumor volumes were measured at 5-, 10-, 15, 20-, and 25-days post-injection by determining the length and width of the tumors with a slide gauge. After 30 days, the mice were sacrificed, and the tumors were excised, photographed, and measured. The collected tumors were processed for immunohistochemical staining. For the metastasis model, the same 36 mice were again randomly divided into three groups: control, shNC, and shNPM1. HK-1 or CNE3 cells (5×105 cells in 150 µL PBS) infected without (control) or with adenovirus-carrying shNC or shNPM1 were injected into the mice via the tail vein. After 5 weeks, lung samples were collected for pulmonary metastasis assessment.
For Figure 7, 60 mice were randomly assigned to five groups: control, shNC+NC, shNSUN2, YBX1, and shNSUN2+YBX1. HK-1 or CNE3 cells without infection (control) or infected with adenovirus-carrying shNC plus NC, shNSUN2, YBX1, or both shNSUN2 and YBX1 were injected subcutaneously into the right flank of each mouse (1×106 cells in 200 µL PBS per mouse). Tumor volumes were recorded at 5-, 10-, 15, 20-, and 25-days days using a slide gauge to measure tumor length and width. After 30 days, the mice were sacrificed, and the tumors were excised, photographed, and measured. Tumor samples were collected for immunohistochemical analysis. To establish a metastasis model, the 60 mice were divided into the same five groups: control, shNC+NC, shNSUN2, YBX1, and shNSUN2+YBX1. The

control group received HK-1 or CNE3 cells without infection, while the shNC+NC group received HK-1 or CNE3 cells infected with adenovirus-carrying shNC and NC (5×105 cells in 150 µL PBS). The shNSUN2, YBX1, and shNSUN2+YBX1 groups received HK-1 or CNE3 cells infected with adenovirus-carrying shNSUN2, YBX1, or both shNSUN2 and YBX1, respectively (5×105 cells in 150 µL PBS for each group). All injections were administered via the tail vein. After 5 weeks, lung samples were harvested for the detection of pulmonary metastasis.

Immunohistochemical (IHC) staining

Tumor samples from NPC were fixed in 3.7% buffered formalin and subsequently embedded in paraffin. IHC analysis was performed on tissue sections with a thickness of 5 µm, which were prepared from the paraffin-embedded blocks. The sections underwent deparaffinization and rehydration, followed by antigen retrieval through heat-induced epitope recovery in citrate buffer. To inhibit endogenous peroxidase activity, the sections were treated with hydrogen peroxide. Afterward, the tissue sections were pre-incubated with goat serum to block nonspecific binding sites, then incubated overnight at 4°C with primary antibodies targeting Ki67 (Thermo Fisher Scientific, Cat. No. MA5-14520, 1:100), NSUN2 (Thermo Fisher Scientific, Cat. No. PA5-115674, 1:100), YBX1 (Thermo Fisher Scientific, Cat. No. PA5-83493, 1:100), NPM1 (Thermo Fisher Scientific, Cat. No. 32-5200, 1:500), and PKM2 (Thermo Fisher Scientific, Cat. No. PA5-28700, 1:100). After washing with PBS, the sections were incubated with secondary antibodies at room temperature for 1 hour. Hematoxylin was applied as a counterstain before the sections were mounted and examined using a DMi8 optical microscope.

Immunofluorescent (IF) staining

The NPC tumor sections underwent deparaffinization and rehydration, followed by antigen retrieval through heat-induced epitope recovery using citrate buffer. To block nonspecific binding, the sections were incubated at room temperature for 1 hour in a solution containing 1% bovine serum albumin. After blocking, the samples were treated overnight at 4°C with primary antibodies targeting PKM2 (Abcam, Cat. No. ab85555, 1:200) and NPM1 (Abcam, Cat. No. ab10530, 1:500). The next day, the sections were rinsed three times with PBS and then incubated with the appropriate secondary antibodies (Abcam) for 2 hours at room temperature. For nuclear staining, 4¦,6- diamidino-2-phenylindole (DAPI) from Life Technologies (Waltham, CA, USA) was applied. Fluorescent imaging of the labeled cells was performed using a ZEISS fluorescence microscope.

Metabolic analysis

Mitochondrial respiration and glycolysis were assessed using the Seahorse XF96 flux analyzer (Agilent Technologies, Santa Clara, USA). To begin, cells were plated at a density of 20,000

cells per well in XF96 culture plates and incubated overnight to allow cell attachment. The next day, the cells were exposed to 3 mM metformin hydrochloride for 48 hours before performing the metabolic analysis. Before initiating the mitochondrial respiration assay, the growth medium was replaced with an unbuffered, serum-free DMEM solution, containing 8.3 g/L DMEM (D5030, Sigma- Aldrich), 1.85 g/L NaCl (Sigma-Aldrich), 2 mM L-glutamine (Corning), and glucose at the concentration specified in the experimental conditions. For the glycolysis assays, glucose-free media was used. The plates were incubated for 1 hour at 37°C in a CO2- free incubator before the assay. Both Oxygen Consumption Rate (OCR) and Extracellular Acidification Rate (ECAR) were measured over 96 minutes (15 cycles of mixing and measuring), with compounds being injected at intervals of three cycles. For the glycolysis assays, the following compounds (Sigma-Aldrich) were added sequentially to the wells, with the final concentrations being glucose (10 mM), oligomycin (3 µM), CCCP (0.25 µM), and 2-deoxy-D-glucose (100 mM). For the mitochondrial respiration assays, the compounds injected sequentially (with final concentrations in the wells) were: oligomycin (3

µM), CCCP (0.25 µM), rotenone (1 µM), and antimycin A (1 µM). Basal respiration was determined by subtracting post- injection respiration with antimycin A from baseline respiration. ATP production was calculated as the difference between baseline respiration and respiration after oligomycin injection. Maximal respiratory capacity was determined by CCCP- stimulated respiration minus antimycin A-inhibited respiration. Spare respiratory capacity was calculated by subtracting baseline respiration from CCCP-stimulated respiration. Protein concentration in each well was measured for normalization using the Pierce BCA Protein Assay (ThermoFisher Scientific), following the manufacturer's instructions.

Bioinformatics prediction
BioGRID (https://thebiogrid.org/) predicted that NPM1 bound to PKM2. RM2Target (http://rm2target.canceromics.org/) identified NSUN2 and NSUN6 as m5C writer proteins that interacted with PM1. Additionally, RM2Target (http://rm2target.canceromics.org/) predicted m5C reader proteins YBX1 and ALYREF, as interacting with NPM1.
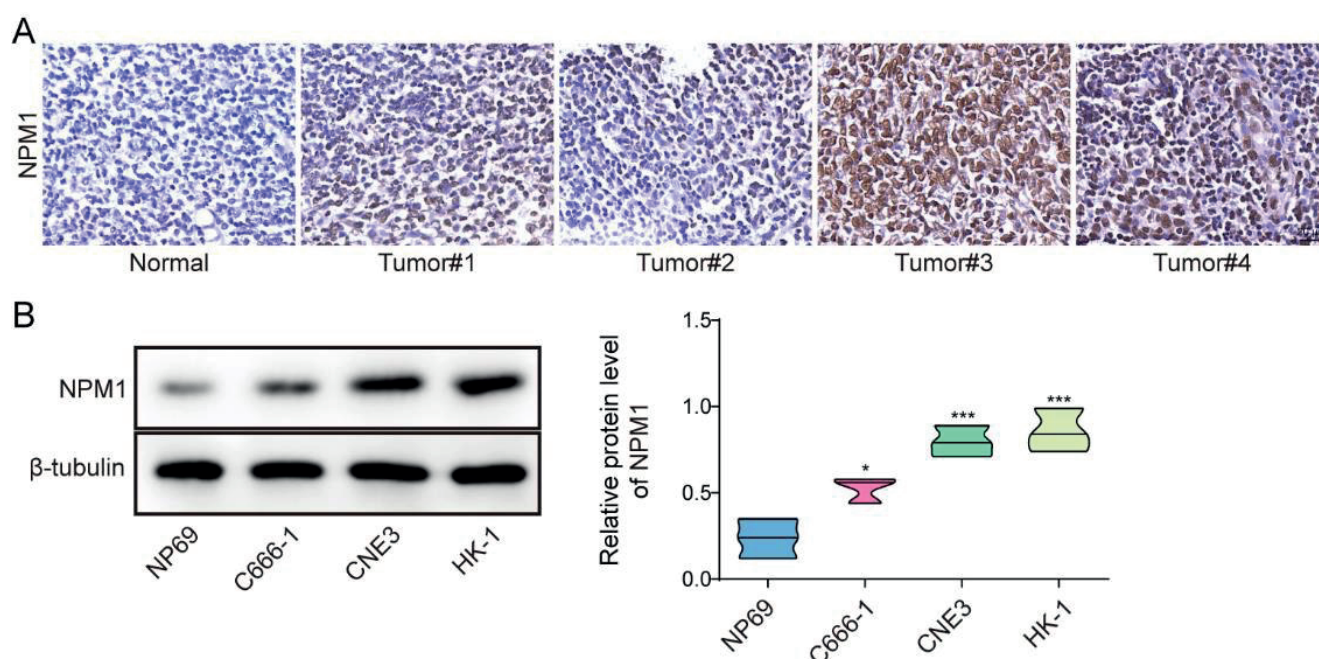

Figure S1. NPM1 was highly expressed in nasopharyngeal carcinoma tissues and cells. NPM1 expression was evaluated by immunohistochemistry (IHC) in different grades of NPC tissues and normal nasopharyngeal tissues (n=5 for each group). Scale bar = 20 µm. A) NPM1 expression was assessed by Western blot in the normal nasopharyngeal epithelial cell line (NP69) and NPC cell lines (CNE3, HK-1, and C666-1). Unless specified otherwise, n=3. *p<0.05, ***p<0.001.
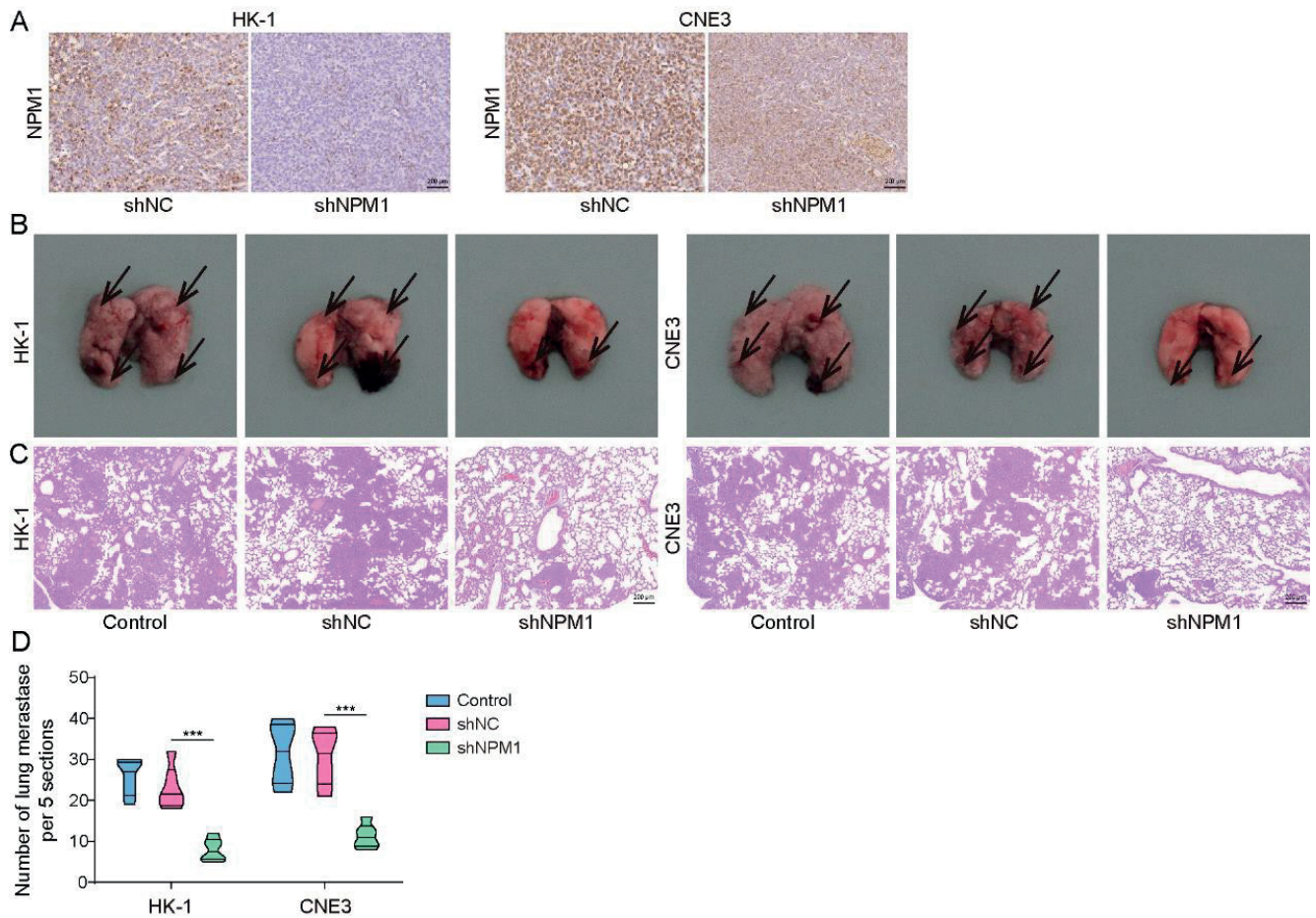
Figure S2. Expression of NPM1 and its role in lung metastasis of NPC cells in nude mice. A) Immunohistochemistry (IHC) was performed to detect the expression of NPM1 in the NPC from the nude mice. Scale bar = 200 μm. n=6. B-D) NPM1-knockdown and control NPC cells were injected via the tail vein into nude mice. Afterward, the lung metastasis and nodule formation were assessed. Scale bar = 200 μm. n=6. ***p<0.001.
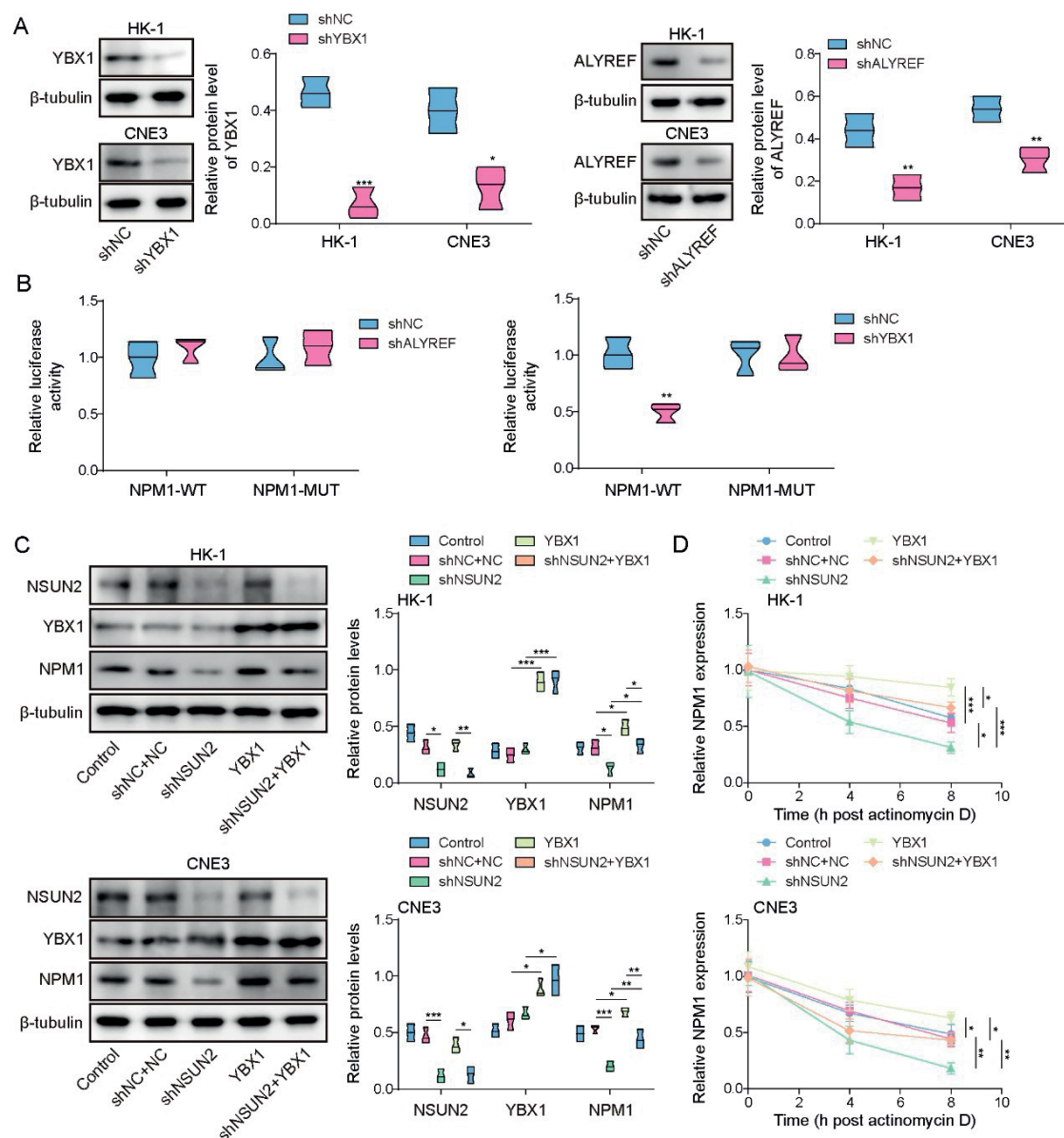
Figure S3. Roles of YBX1, ALYREF, and NSUN2 in regulating NPM1 expression and mRNA stability in NPC cells. A) YBX1 and ALYREF were knocked down in NPC cell lines and Western blot was used to assess their expression levels. B) The dual-luciferase reporter assay was conducted to determine the binding of m5C readers YBX1 and ALYREF to m5C sites on NPM1 mRNA. C) NPC cells with NSUN2 knockdown and/or YBX1 overexpression were generated, and Western blot analysis was performed to detect the expression levels of NSUN2, YBX1, and NPM1. D) The stability of NPM1 mRNA was analyzed by RT-qPCR after treatment with actinomycin D. Unless specified otherwise, n=3. *p<0.05, **p<0.01, ***p<0.001.
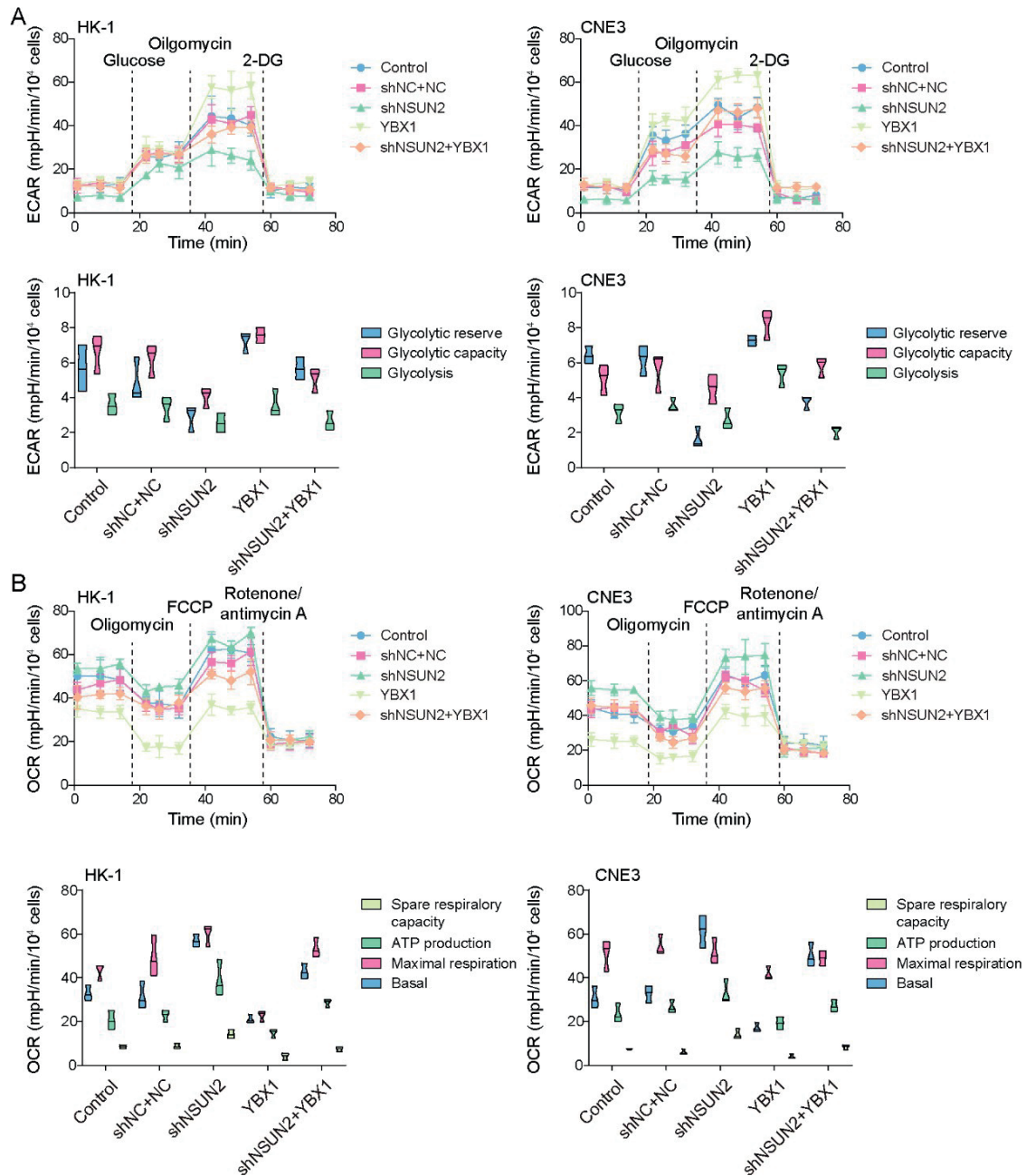
Figure S4. Assessment of glycolytic activity and oxidative phosphorylation in NPC cells. A) Extracellular acidification rate (ECAR) analysis was conducted using an XF96 metabolic analyzer to assess changes in glycolytic activity, including glycolytic capacity, basal glycolysis rate, and maximum glycolysis rate. B) Oxygen consumption rate (OCR) analysis was performed using an XF96 metabolic analyzer to evaluate levels of oxidative phosphorylation (OXPHOS), including basal respiration, maximal respiration, ATP production, and spare respiratory capacity.